ARTICLE

Social isolation reinforces aging-related behavioral inflexibility by promoting neuronal necroptosis in basolateral amygdala

Juan Zhang[1,8], Dan Liu[2,8], Peng Fu[3,8], Zhi-Qiang Liu[1], Chuan Lai[1], Chun-Qing Yang[1], Kai Chen[1], Wen-Dai Bao[1], Fan Hu[1], Hui-Yun Du[4], Weili Yang[5], Jie Wang[6], Heng-Ye Man[7], Youming Lu[1] and Ling-Qiang Zhu[1]✉

Aging is characterized with a progressive decline in many cognitive functions, including behavioral flexibility, an important ability to respond appropriately to changing environmental contingencies. However, the underlying mechanisms of impaired behavioral flexibility in aging are not clear. In this study, we reported that necroptosis-induced reduction of neuronal activity in the basolateral amygdala (BLA) plays an important role in behavioral inflexibility in 5-month-old mice of the senescence-accelerated mice prone-8 (SAMP8) line, a well-established model with age-related phenotypes. Application of Nec-1s, a specific inhibitor of necroptosis, reversed the impairment of behavioral flexibility in SAMP8 mice. We further observed that the loss of glycogen synthase kinase 3α (GSK-3α) was strongly correlated with necroptosis in the BLA of aged mice and the amygdala of aged cynomolgus monkeys (*Macaca fascicularis*). Moreover, genetic deletion or knockdown of GSK-3α led to the activation of necroptosis and impaired behavioral flexibility in wild-type mice, while the restoration of GSK-3α expression in the BLA arrested necroptosis and behavioral inflexibility in aged mice. We further observed that GSK-3α loss resulted in the activation of mTORC1 signaling to promote RIPK3-dependent necroptosis. Importantly, we discovered that social isolation, a prevalent phenomenon in aged people, facilitated necroptosis and behavioral inflexibility in 4-month-old SAMP8 mice. Overall, our study not only revealed the molecular mechanisms of the dysfunction of behavioral flexibility in aged people but also identified a critical lifestyle risk factor and a possible intervention strategy.

Molecular Psychiatry; https://doi.org/10.1038/s41380-022-01694-5

INTRODUCTION

Behavioral flexibility, a core adaptive function of the executive control system in the brain, is the ability to flexibly adjust one's behavior according to the changing environment [1]. It enables individuals, governments and institutions to quickly and properly respond to unpredictable circumstances such as the global COVID-19 pandemic. Flexibility promotes executive function development during emerging adulthood [2, 3] and can alleviate the impact of aging on cognitive decline [4]. Numerous studies have suggested that the neurobiological basis of behavioral flexibility is the ability of some key brain regions to flexibly reconfigure themselves in response to changing demands [5]. Neurons in the basolateral amygdala (BLA) receive input and output from posterior piriform cortex (PPC) or orbitofrontal cortex (OFC) in the circuitry that drives responses to changed odor cues in a reversal learning task [6–8]. Circuits containing axonal projections from the BLA to the nucleus accumbens (NAc), OFC or medial prefrontal cortex (mPFC) neurons play unique roles in altering behavioral responses when a cue is devalued [9–13]. These data suggest that the BLA might be a critical brain area for integrating previous information with new changes in odor cues or delay time to appropriately alter behavior. Flexibility deficits have been reported in many neuropsychiatric disorders, such as autism, schizophrenia, obsessive-compulsive disorder (OCD), and late-onset dementias [5]. Normal aging is usually associated with many cognitive and neurobiological deficits, including behavioral rigidity and cognitive inflexibility [1]. Impairment of reversal learning in elderly people is a behavioral pattern in which subjects are slow to recognize and learn from shifts in rewards. Delay-based flexible decision-making is impaired in old age, in that the subject loses the ability to recognize the reduced value of the delayed reward and learn to switch to an alternative [14]. Elderly adults, aged rats and older monkeys exhibited impaired reversal learning [15–17]. They also showed impaired flexibility in the delay discounting task, shifting behavior away from the delayed reward more slowly than younger mice [18, 19]. However, the underlying mechanisms remain elusive.

[1]Department of Pathophysiology, Key Lab of Neurological Disorder of Education Ministry, School of Basic Medicine, Tongji Medical College, Huazhong University of Science and Technology, Wuhan, China. [2]Department of Medical Genetics, School of Basic Medicine, Tongji Medical College, Huazhong University of Science and Technology, Wuhan, China. [3]Department of Neurosurgery, Union Hospital, Huazhong University of Science and Technology, Jiefang Avenue No. 1277, 430022 Wuhan, China. [4]Department of Physiology, School of Basic Medicine, Tongji Medical College, Huazhong University of Science and Technology, Wuhan, China. [5]Guangdong Key Laboratory of Non-human Primate Research, Guangdong Hongkong-Macau Institute of CNS Regeneration, Jinan University, Guangzhou 510632, China. [6]Key Laboratory of Magnetic Resonance in Biological Systems, State Key Laboratory of Magnetic Resonance and Atomic and Molecular Physics, National Center for Magnetic Resonance in Wuhan, Wuhan Institute of Physics and Mathematics, Innovation Academy for Precision Measurement Science and Technology, Chinese Academy of Sciences-Wuhan National Laboratory for Optoelectronics, Wuhan, Hubei 430071, China. [7]Department of Biology, Boston University, Boston, MA 02215, USA. [8]These authors contributed equally: Juan Zhang, Dan Liu, Peng Fu
✉email: zhulq@mail.hust.edu.cn

Received: 31 January 2022 Revised: 28 June 2022 Accepted: 30 June 2022
Published online: 15 July 2022

Neuronal loss is one of the most prominent pathological hallmarks of aging and plays an important role in aging related cognitive decline [20, 21]. The massive loss of neurons in the human subiculum and the hilus of the dentate gyrus is associated with the decline of relational memories in aging, which may impair the functional integrity of brain regions closely involved in memories [22]. Atrophy of the entorhinal cortex due to neuronal loss significantly correlated with performance on clinical cognitive tests in elderly subjects prior to the onset of dementia [23]. Loss of hippocampal neurons is associated with memory impairments in SAMP8 mice [24]. Neuronal loss in the hippocampus and cerebral neocortex leads to degenerative pathological changes in Alzheimer's disease (AD), which, in turn, affect cognitive ability [25, 26]. Apoptosis and necroptosis are the two main types of programmed cell death in the aged brain [27]. Apoptosis occurs in the aging process, and contributes to aging-related pathologies [28]. Necroptosis is activated in the brains of aged mice and increases with age [29]. Inhibition of necroptosis mitigates retinal degeneration in age-related macular degeneration (AMD) [30] and prolongs the survival time of age-related atherosclerosis model mice [31]. The activation of necroptosis not only causes neuronal loss in AD mouse models [32], but also drives the loss of motor neurons derived from human embryonic stem cells in a humanized in vitro model of amyotrophic lateral sclerosis (ALS) [33]. In addition, it is a key factor that induces dopaminergic neuron loss in Parkinson's disease (PD) models [34]. Both apoptosis and necroptosis can exacerbate cognitive deficits in mouse models [32, 35]. However, it is not clear whether programmed cell death is involved in the changes in behavioral flexibility in aged animals.

Here, by c-fos/Egr1 staining and electrophysiological recording, we found that 5-month-old SAMP8 mice displayed dysfunction of behavioral flexibility, accompanied by a reduction in neuronal activity in the BLA. Further study suggested that the loss of neurons caused by RIPK3-dependent necroptosis but not apoptosis in the BLA played a key role in the behavioral inflexibility in aged mice. With a combination of microarray screening, we reported that decrease in GSK-3α was positively correlated with neuronal necroptosis in aged mice and aged cynomolgus monkeys. Moreover, the loss of GSK-3α led to neuronal necroptosis and behavioral inflexibility, whereas overexpression of GSK-3α ameliorated these abnormalities in aged mice. We demonstrated that GSK-3α regulated RIPK3-dependent necroptosis via regulation of the mTORC1 signaling pathway. Finally, social isolation (living alone), a common social phenomenon among older people, could accelerate necroptosis in the BLA and behavioral inflexibility in aged mice.

RESULTS

SAMP8 mice display impaired behavioral flexibility and impaired behavioral flexibility was correlated with the inactivation of the BLA

Previous studies revealed that SAMP8 mice displayed cognitive impairments as early as 4–6 months of age [36]. We then examined behavioral flexibility in SAMP8 mice starting at 5 months by employing a classic reversal learning behavioral paradigm (Fig. 1A, B) and a previously reported delay discounting protocol [37] with minor modifications (Fig. 1E). As indicated, 5-month-old SAMP8 mice needed more trials to reach criterion during reversal and made more regressive errors than their controls (senescence-accelerated mouse resistant 1, SAMR1) (Fig. 1C, D) in the reversal learning paradigm. SAMP8 mice display comparable probability of choosing the high-reward arm (HRA) with SAMR1 mice during the acquisition phase with no delay but a much higher probability of choosing the HRA when the delay time was set at 5 s and 10 s (Fig. 1F, G), suggesting a reduced behavioral flexibility in delay discounting task and shifting behavior away from the delayed reward more slowly than SAMR1 mice. Simultaneously, SAMP8 mice did not show any difference from SAMR1 mice in the open-field test (OFT), elevated plus maze task (EPM) or novel object recognition test (NORT), but reduced freezing time in contextual fear memory (FCT) task (Supplementary Fig. 1A, K), indicating intact locomotor ability, normal working memory, no anxious behavior but impaired contextual fear memory.

The OFC, Amy and PPC are three important brain regions for odor-based reversal learning [6], and the mPFC, OFC, NAc and Amy are involved in delay discounting behavior [12, 38, 39] (Fig. 1H). We therefore performed c-fos and Egr1 staining to examine neuronal activity in the OFC and amygdala because they are implicated in the above two behavioral flexibility paradigms. We found that the intensity of c-fos and Egr1 was reduced dramatically in the BLA but not in the other brain areas (Fig. 1H–J, Supplementary Fig. 2A–E), suggesting the possible involvement of the BLA in mediating behavioral flexibility in SAMP8 mice. To further explore the role of BLA neuronal activity in behavioral flexibility, mice were allowed to record spontaneous local field potential (LFP) activity in the BLA during odor-based reversal learning. We found that LFP power (theta, 4–12 Hz) was decreased in the pre-learning and learnt stages during the reversal process in SAMP8 mice (Fig. 1K–P), suggesting that the theta oscillations of neuronal clusters were weakened in the BLA of SAMP8 mice. Decreased oscillations of neuronal clusters indicated impaired function or reduced activity of neurons, which was consistent with the downregulation of c-fos and Egr1 levels in the BLA. In addition, we found a compensatory increase in theta oscillations of neuronal clusters in the BLA during the learning phase of reverse learning (Fig. 1P). Besides, our results showed that SAMP8 mice spent more time in the learning phase of each trial (Fig. 1Q), which showed that compensatory increases in theta oscillations of BLA neuron clusters during the learning phase contribute to the learning process in SAMP8 mice but do not improve flexibility behavioral deficits.

Impaired behavioral flexibility is caused by the activation of neuronal necroptosis in the BLA of aged mice

We then queried whether the decreased theta oscillations of neuronal clusters and downregulation of c-fos levels were due to the loss of firing neurons in the BLA. We employed Nissl's staining and immunohistochemistry with synaptophysin (SYP) and NeuN to examine the neuron and synapse density and found visible neuronal loss and decreased intensity of SYP in the BLA of SAMP8 mice (Fig. 2A–C, Supplementary Fig. 3A, B). Furthermore, we examined inflammatory biological phenotypes associated with aging and found that the proinflammatory factors (IL-6, TNF-α, IL-1β) were not increased in the amygdala of SAMP8 mice (Supplementary Fig. 4A). Interestingly, apparent neuron loss in the amygdala of 25-year-old cynomolgus monkey compared with 8-year-old cynomolgus monkey was also found (Fig. 2D–F). Therefore, we hypothesized that reduced the number of firing neurons in the BLA impaired behavioral flexibility in SAMP8 mice. As apoptosis and necroptosis are the two main types of cell death in the aged brain [27], we then wanted to determine which form of cell death plays a vital role in the neuronal loss of BLA. We excluded apoptosis because the levels of cleaved-PARP1, cleaved-Caspase-8 and TUNEL$^+$ neurons were comparable between the SAMP8 and SAMR1 mice (Supplementary Fig. 5A–D). However, the levels of RIPK3, pRIPK3, MLKL and pMLKL but not RIPK1 were much higher in the BLA of SAMP8 mice than in that of control mice, indicating RIPK1-independent necroptosis (Fig. 2G, H). Moreover, the membrane translocation of pMLKL, a critical step for necroptosis, was apparent in the BLA neurons of SAMP8 mice (Fig. 2I, J). The same phenomenon has also been observed in the amygdala of aged cynomolgus monkeys (Fig. 2K, L). Additionally, by treating

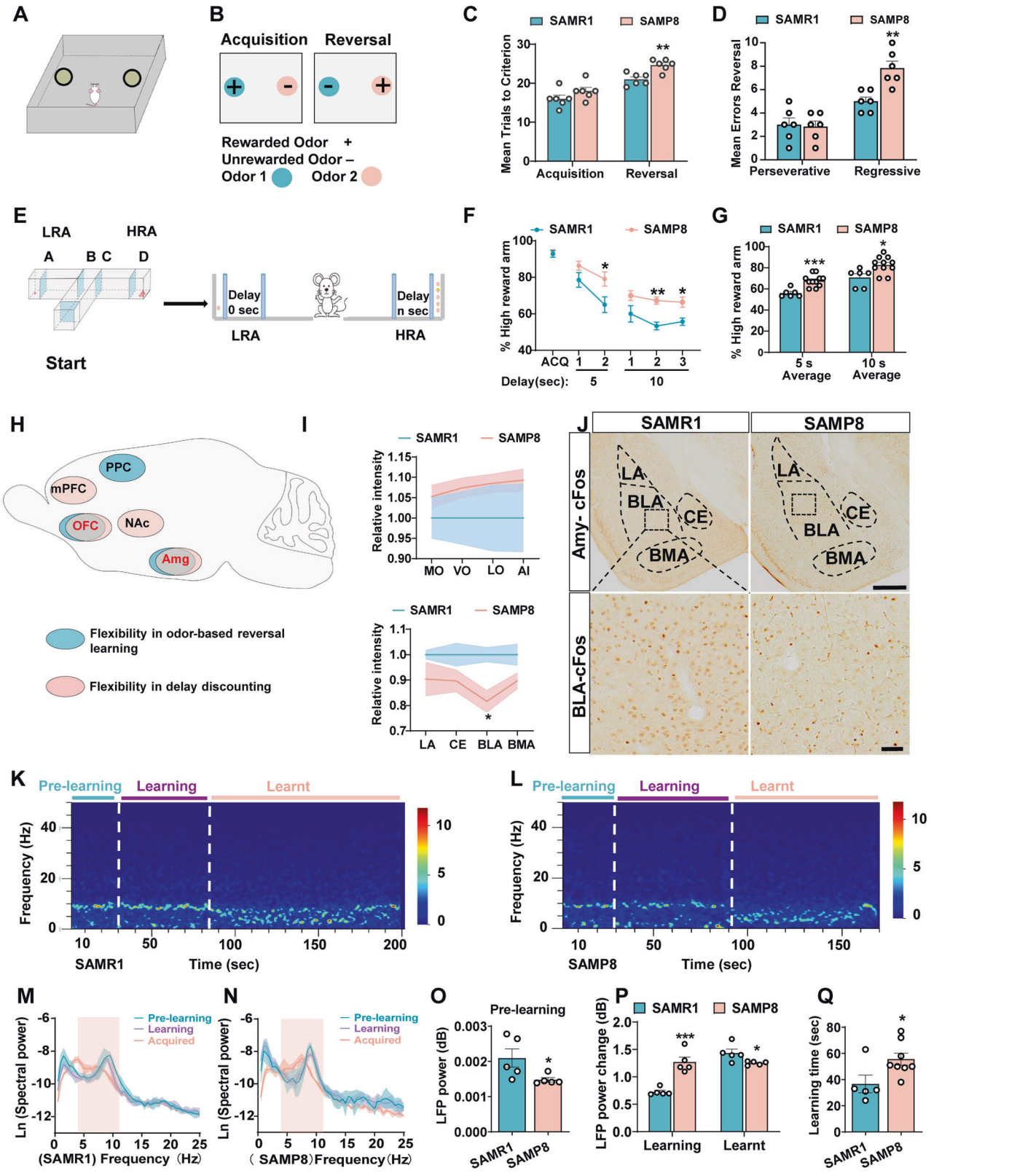

SAMP8 mice with Nec-1s, a selective inhibitor of necroptosis [34], we found that neuronal necroptosis in the BLA (Supplementary Fig. 6A, B) and behavioral flexibility was significantly alleviated in SAMP8 mice (Fig. 2M–P). No apparent alteration was found in the OFT or EPM (Supplementary Fig. 6C–F). Collectively, these data strongly demonstrated that necroptosis, but not apoptosis played an important role in mediating neuronal loss and behavioral flexibility in aged mice.

Fig. 1 Impaired behavioral flexibility is correlated with reduced neuronal activity in the BLA of SAMP8 mice at 5-month. Schematic diagram of the apparatus (**A**) and behavioral process (**B**) for odor-based reversal learning experiment. The mean number of trials to reach criterion during acquisition and reversal for 5-month-old SAMP8 and the age matched control mice (SAMR1) (**C**), the mean number of perseverative and regressive errors during reversal for SAMP8 and SAMR1 mice (**D**). (**E**) Schematic diagram of the behavioral process and apparatus for delay-based flexible discounting experiment. The percentage of high-reward arm (HRA) chosen during acquisition stage (ACQ) or when the delay time was set at 5 s and 10 s for 5-month-old SAMP8 and the age matched SAMR1 mice (**F**), the percentage mean of HRA chosen when the delay time was set at 5 s and 10 s (**G**). Schematic diagram of brain regions involved in flexibility behaviors (**H**), the relative optical intensity of c-fos in different brain regions was analyzed by Image (**I**). Immunochemical staining of c-fos in the different sub-regions of amygdala (**J**) from age matched SAMR1 and SAMP8 mice (Bar = 500 μm, Amy; Bar = 50 μm, BLA). Representative LFP spectrograms of 5-month-SAMR1 mice (**K**) and 5-month-SAMP8 mice (**L**) in different behavioral stage during reversal learning, LFP spectral powers were expressed in frequency domain from 0 to 25 Hz in 5-month-SAMR1 mice (**M**) and 5-month-SAMP8 mice (**N**), the pink shade marked the frequency domain used for quantitative comparison of LFP powers from 4 to 12 Hz. LFP powers (theta, 4–12 Hz) were statistically analyzed in the stage of pre-learning during reversal process in 5-month-SAMR1 mice and 5-month-SAMP8 mice (**O**). The change of LFP powers (4–12 Hz) in the stage of learning and learnt were measured relative to 30 sec baseline segments (pre-learning phase) in SAMR1 mice and SAMP8 mice (**P**). The learning time was analyzed in the phase of learning during reversal between SAMR1 mice and SAMP8 mice (**Q**). $^{*}p < 0.05$, $^{**}p < 0.01$, $^{***}p < 0.001$, *vs* SAMR1 mice (Data are represented as mean ± SEM; Unpaired *t* test, multiple *t* test adjusted with Holm-Sidak and two-way ANOVA with Sidak post hoc comparison test; $n = 4$~11 for each group).

The reduction of GSK-3α is correlated with necroptosis, and inhibition of GSK-3α in the BLA leads to necroptosis and accelerated the impairment of the behavioral flexibility

We then wanted to explore the underlying molecular mechanisms that mediated necroptosis in the BLA of aged mice. To this end, we performed mRNA microarrays on the amygdala from 5-month-old SAMR1 and SAMP8 mice. We found that eight genes were significantly downregulated ($p < 0.05$, fold change ≥ 2.0) in SAMP8 mice (Fig. 3A). Among these 8 down-regulated genes (GSK-3α, Fos, Egr2, Sag, Upk1b, Neurod4, Actrt1, 4930583H14Rik), GSK-3α is the only gene reported to be involved in aging-related pathological regulation and cell death [40, 41], Moreover, the mRNA and protein levels of GSK-3α but not GSK-3β was decreased in the BLA of SAMP8 mice (Fig. 3B–G). In line with it, the reduction of GSK-3α can also be found in the amygdala of aged cynomolgus monkey (Fig. 3H–I). Given the critical role of GSK-3α in aging-related pathologies [42], we then queried whether the loss of GSK-3α, which participated in the necroptosis, induced neuronal loss and behavioral flexibility in aged mice. We examined the protein levels of GSK-3α/β, NeuN-positive neurons, and necroptosis-related molecules in the amygdala of SAMP8 mice at 3, 5, 8, and 10 months. We found that the reduction in GSK-3α but not GSK-3β and the loss of NeuN-positive neurons were prominent from 5 months. Meanwhile, the levels of GSK-3α and NeuN gradually decreased with age in SAMP8 mice (Supplementary Fig. 7A–G). The expression of RIPK3, pRIPK3, MLKL, pMLKL but not RIPK1 increased from 5 to 10 months (Supplementary Fig. 7H–J). Moreover, the decrease in GSK-3α in BLA was highly correlated with the membranous shift of pMLKL (Fig. 3J–N), a critical step of necroptosis [32]. No significant correlation was found between GSK-3α and caspase-3, an indicator of apoptosis (Supplementary Fig. 7K, L). Therefore, we hypothesized that decreasing GSK-3α might play an important role in the necroptosis of BLA neurons in aged mice.

We then asked whether the loss of GSK-3α played an important role in the necroptosis of BLA and behavioral flexibility in aged mice. We generated a mouse model with neuron-specific GSK-3α knockout in the BLA (GSK-3α$^{+/-}$) by injecting the adeno-associated virus (AAV2/8) -packaged Cre recombinase fused with EGFP or EGFP only into the BLA of GSK-3α$^{flox/+}$ mice (Fig. 3O,P) [43]. Immunofluorescence data suggested that this strategy for knockout was successful because the intensity of GSK-3α was dramatically reduced in the EGFP positive neurons of BLA (Fig. 3q). Meanwhile, no differences on the body and brain in weight and size were found between the GSK-3α$^{+/-}$ and GSK-3α$^{+/+}$ mice (Supplementary Fig. 8a, b). We also found that the levels of RIPK3, pRIPK3, MLKL and pMLKL were increased in the BLA of GSK-3α$^{+/-}$ mice, and no significant changes were found in the expression of GSK-3β between the two groups (Fig. 3r-s). Additionally, the elevation of RIPK3, MLKL and pMLKL are more prominent in the EGFP positive neurons and positively correlated with the EGFP intensity (Fig. 3T, U). Furthermore, by using a short hairpin RNA (shRNA) to inhibit the GSK-3α (Sh-GSK-3α), we also detected the activation of necroptosis in the BLA (Supplementary Fig. 9A–D). Thus, loss of GSK-3α by artificial approaches in the BLA led to the necroptosis. We then subjected the mice with GSK-3α inhibition to the behavioral flexibility test and found that both GSK-3α$^{+/-}$ mice and Sh-GSK-3α mice displayed the impairment of the behavioral flexibility (Fig. 3V–Y; Supplementary Fig. 9E–H). To elucidate the specific role of GSK-3α in necroptosis and behavioral inflexibility, we specifically knocked down GSK-3β in the BLA of wild-type mice *via* a specific shRNA against GSK-3β, the results showed GSK-3β knockdown had no effect on the necroptosis and behavioral flexibility (Supplementary Fig. 9I–M). Additionally, overexpression of Bmp15, the most upregulated gene in the BLA of SAMP8 mice, did not impair the behavioral flexibility (Supplementary Fig. 10A-I).

When administrating Nec-1s to the GSK-3α$^{+/-}$ mice with reduced GSK-3α, we found that the impaired behavioral flexibility was rescued in GSK-3α$^{+/-}$ mice treated with Nec-1s (GSK-3α$^{+/-}$-Nec-1s) (Supplementary Fig. 11A–F) and necroptosis was alleviated in the BLA in GSK-3α$^{+/-}$-Nec-1s group (Supplementary Fig. 11G, H). No significant changes were found in the locomotor and anxious behavior in these mice (Supplementary Fig. 12A–L). Taken together, these data demonstrated that reduction of GSK-3α in the BLA resulted in the necroptosis and the impairment of the behavioral flexibility in aged mice.

Overexpression of GSK-3α alleviates necroptosis in the BLA and the impairment of the behavioral flexibility in aged mice, and the mTORC1 signaling mediates the necroptosis induced by GSK-3α loss

We then want to explore whether overexpression of GSK-3α could alleviate the necroptosis in BLA and the dysregulation of behavioral flexibility in aged mice. We injected AAV-GSK-3α, consisting of AAV–packaged full-length mouse GSK-3α complementary DNA (cDNA), into the BLA of SAMP8 mice at 4 months (Fig. 4A–C). We found that the levels of RIPK3, pRIPK3, MLKL, pMLKL but not GSK-3β were dramatically decreased in the BLA of SAMP8 mice with GSK-3α overexpression (Fig. 4D, E). Concomitantly, the RIPK3, MLKL and pMLKL levels were significantly downregulated in the mCherry positive BLA neurons and negatively correlated with the mCherry intensity ((Fig. 4F, G). In addition, overexpression of GSK-3α in the BLA can alleviate the behavioral flexibility (Fig. 4H–K), and no significant changes were found in the OFT and the EPM (Supplementary Fig. 13A–D). Taken together, these findings demonstrated that overexpression of GSK-3α in BLA alleviated the necroptosis and behavioral flexibility in aged mice.

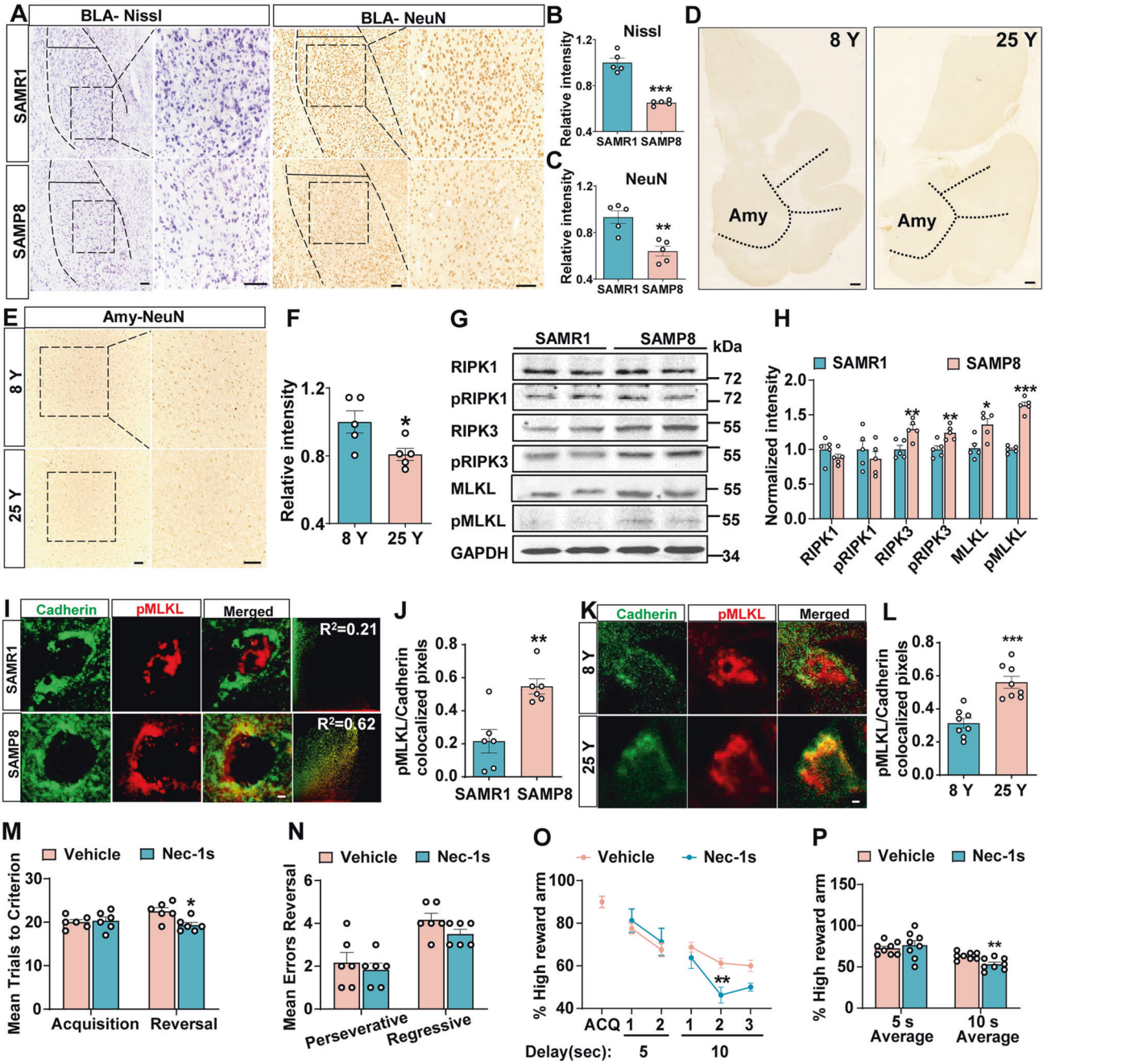

Fig. 2 Impaired behavioral flexibility is due to the increased necroptosis in the BLA of aged mice. The Nissl staining and immunochemical staining of NeuN (Bar = 100 μm) in the BLA from age matched (5 months) SAMR1 and SAMP8 mice. The representative images were shown in **A** and the quantitative analysis of Nissl staining was performed in **B** the relative optical intensity of NeuN was shown in panel **C**. **D** Representative immunofluorescence images in the whole brain stained with anti-NeuN antibody in 8-year-old (8 Y, left) and 25-year-old (25 Y, right) cynomolgus monkeys (Bar = 2 mm). Coronal slices from 8-year-old and 25-year-old cynomolgus monkeys were stained with anti-NeuN (Bar = 100 μm). The representative images were shown in **E** and the quantitative analysis was performed by Image J (**F**). **G**, **H** The protein levels of RIPK1, pRIPK1 (S166), RIPK3, pRIPK3 (T231/S345), MLKL, and pMLKL (S345) were measured by western blotting and the quantitative analysis was performed in **H**. The brain sections from SAMR1 and SAMP8 mice at 5 months were immunostained with anti-Cadherin (Green) and anti-pMLKL (Red) antibodies (**I**) and the quantitative analysis of co-localized pixels was evaluated by Pearson's correlation (**J**) (Bar = 2 μm). The amygdala sections from 8-year-old and 25-year-old cynomolgus monkeys were immunostained with anti-Cadherin (Green) and anti-pMLKL (Red) antibodies (**K**) and the quantitative analysis of colocalized pixels was evaluated by Pearson's correlation (**L**) (Bar = 2 μm).The mean number of trials to reach criterion during acquisition and reversal for SAMP8 intraperitoneally injected with Nec-1s or the vehicle (**M**), the mean number of perseverative and regressive errors during reversal (**N**). The percentage of HRA chosen during acquisition test or when the delay time was set at 5 s and 10 s from SAMP8 mice intraperitoneally injected with Nec-1s or the vehicle (**O**), the percentage mean of HRA chosen from SAMP8 mice intraperitoneally injected with Nec-1s or the vehicle when the delay time was set at 5 s and 10 s (**P**). $^{*}p < 0.05$, $^{**}p < 0.01$, $^{***}p < 0.001$, vs SAMR1 mice or 8-year-old monkey (for panel **F**), or vehicle treated SAMP8 mice (for panels **M**–**P**) (Data are represented as mean ± SEM; Unpaired *t* test, multiple t test adjusted with Holm-Sidak and two-way ANOVA with Sidak post hoc comparison test; $n = 5$–11 for each group; $n = 5$ brain sections for monkey).

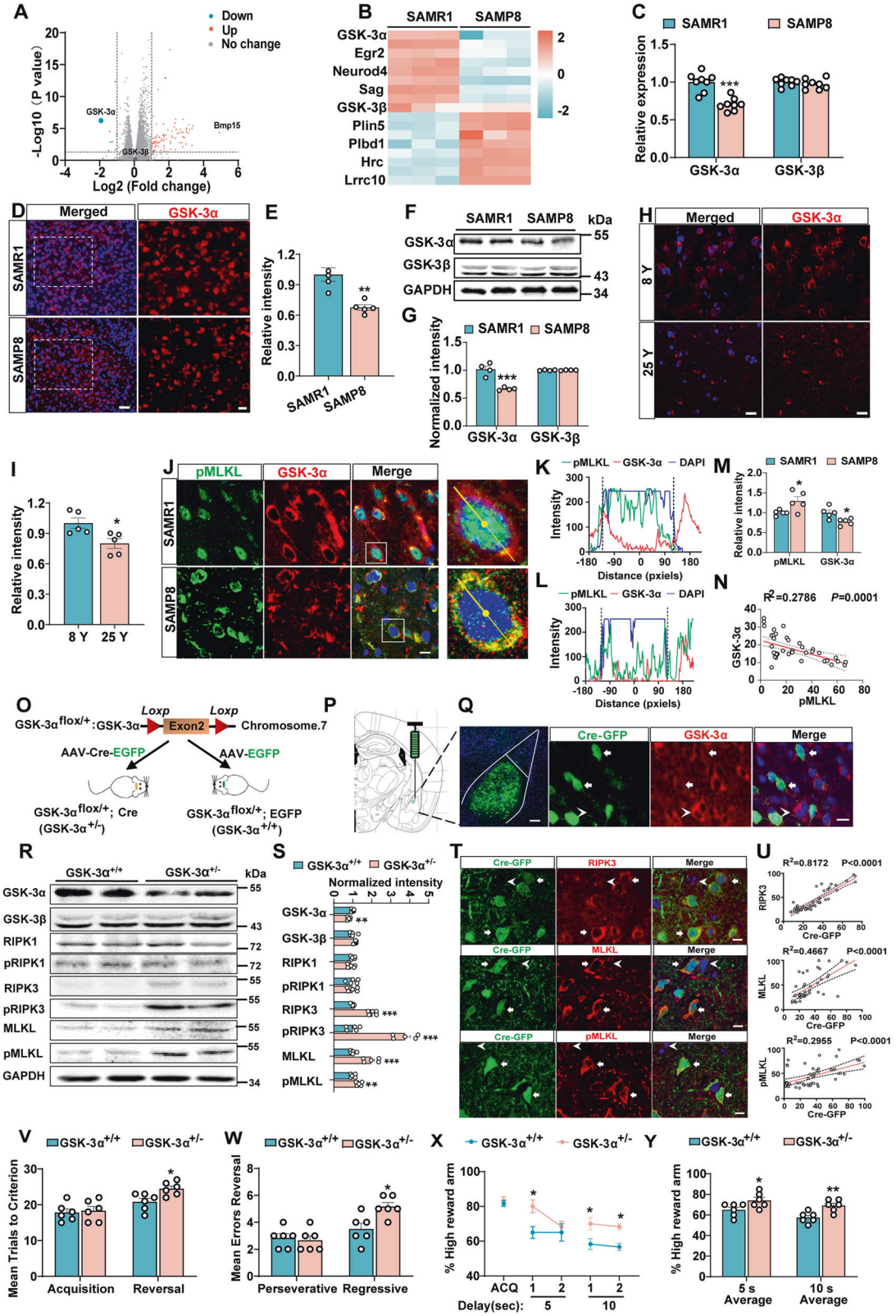

We then asked how the loss of GSK-3α led to the necroptosis in aged mice. We noticed that the total and phosphorylated RIPK3 was significantly upregulated in aged and GSK-3α$^{+/-}$ mice, and downregulated in GSK-3α overexpressing mice. We then speculated that the elevation of total or phosphorylated RIPK3 played an important role in mediating the neuronal necroptosis when GSK-3α was reduced. To this end, we first examined the levels of total and phosphorylation of RIPK3 at different time points upon transfection of sh-GSK-3α in cultured N2a cells. We found that the total RIPK3 increased from 6 h onward and that

Fig. 3 The reduction of GSK-3α in the BLA led to the activation of necroptosis and impaired behavioral flexibility of aged mice. A Volcano plot showed the differentially regulated genes in the amygdala from 5-month-old SAMR1 and SAMP8 mice with the fold change > 2.0 (Red dots) or <−2.0 (Cyan dots) and *p* value <0.05. GSK-3α/β was highlighted by a bigger cyan/black dot independently. The gray and black dots indicated the unchanged genes. **B** Heatmap showing differential expression of top 16 genes (8 upregulated and 8 downregulated) between SAMR1 and SAMP8 mice. **C** The expression of GSK-3α mRNA and GSK-3β mRNA was detected by quantitative real-time polymerase chain reaction (RT-PCR). Coronal slices from SAMP8 and SAMR1 mice were stained with anti-GSK-3α (Red) and DAPI (Blue) (Bar = 50 μm). The representative images were shown in **D** and the fluorescence intensity was measured and the relative intensity was calculated (**E**). Amygdala homogenates were collected and subjected to western blotting assay by using the antibodies of GSK-3α and GSK-3β (**F**), and quantitative analysis was performed in **G**. Immunofluorescence staining was performed in amygdala sections from 8-year-old and 25-year-old cynomolgus monkeys by using anti-GSK-3α (Red) and DAPI (Blue) antibodies (Bar = 20 μm). The representative images were shown in **H** and the fluorescence relative intensity was calculated in **I**. Immunofluorescence staining was performed in amygdala slices from SAMP8 and SAMR1 mice by using anti-GSK-3α (Red) and anti-pMLKL (Green) antibodies. The representative images were shown in **J** (Bar = 50 μm). The fluorescence intensities of GSK-3α (Red line) and the pMLKL (Green line) of a single cell were analyzed (Right panel) following a straight line from the center of nucleus to the membrane (Left panel) by using Image J software in SAMR1 (**K**) and SAMP8 (**L**) mice. The DAPI fluorescence (Blue line) was used as reference. The pixels between the two black vertical dash lines indicated the nucleus regions. Relative intensities of GSK-3α and pMLKL immunoreactivity were measured by Image J software (**M**) and correlative analysis was performed in **N**. **O** Schematic diagram of the generation of GSK-3$\alpha^{+/+}$ and GSK-3$\alpha^{+/-}$ mice. **P** Diagram (left) and representative image (right) for virus injection into the BLA (Bar = 100 μm). (**Q**) Coronal slices from virus infected (Cre-GFP) BLA were stained with anti-GSK-3α (Red) antibody (Bar = 10 μm). Arrowheads indicated neurons without virus infection; arrows indicated neurons with virus infection. The protein levels of GSK-3α, GSK-3β, RIPK1, pRIPK1, RIPK3, pRIPK3, MLKL and pMLKL in the BLA homogenates from GSK-3$\alpha^{+/-}$ and GSK-3$\alpha^{+/+}$ mice were examined by western blotting. The representative images were shown in **R** and the quantitative analysis was shown in **S**. The immunofluorescence was performed in BLA from the GSK-3$\alpha^{+/-}$ mice by using anti-RIPK3, anti-MLKL, anti-pMLKL antibodies (Red). The representative images were shown in **T** and the correlation analysis was performed in **U**. Arrowheads indicated neurons without virus infected; Arrows indicated neurons with virus infected (Bar = 10 μm).The mean number of trials to reach criterion for GSK-3$\alpha^{+/-}$ and GSK-3$\alpha^{+/+}$ mice during acquisition and reversal (**V**), the mean number of perseverative and regressive errors during reversal (**W**). The percentage of HRA chosen during acquisition test or when the delay time was set at 5 s and 10 s for GSK-3$\alpha^{+/-}$ and GSK-3$\alpha^{+/+}$ mice (**X**), the percentage mean of HRA chosen from GSK-3$\alpha^{+/-}$ and GSK-3$\alpha^{+/+}$ mice when the delay time was set at 5 s and 10 s (**Y**). *$p < 0.05$, **$p < 0.01$, ***$p < 0.001$, vs SAMR1 mice (for panels **C**, **E**, **G** and **M**) or 8-year-old monkey (for panel I), or GSK-3$\alpha^{+/+}$ mice (for panels **S**, **V**–**Y**) (Data are represented as mean ± SEM; Unpaired *t* test, multiple *t* test adjusted with Holm–Sidak test and two-way ANOVA with Sidak post hoc comparison test; $n = n = 4$~8 for each group; $n = 5$ brain sections for monkey; Cell number = 42~51 for panel **U**).

the phosphorylation of RIPK3 increased from 12 h onward upon the silencing of GSK-3α (Fig. 4L, M). However, we didn't observe any difference in the mRNA of RIPK3 (Fig. 4N). These data suggested that the impaired degradation of RIPK3 might involve in the necroptosis induced by GSK-3α reduction. Because activated mTOR signaling has been shown to reduce the degradation of RIPK3 by inhibiting autophagy [44], we then examined the mTOR related signaling molecules. We found that the levels of mTOR, phosphorylation of mTOR, phosphorylation of the three well-known substrates of mTORC1: 4E-BP1, S6 kinase, and ribosomal S6 protein were significantly increased in the BLA of GSK-3$\alpha^{+/-}$ mice. Moreover, the phosphorylation of ULK1 was also increased (Fig. 4O, P), suggesting the activation of mTORC1-signaling and the impaired autophagy pathway in GSK-3$\alpha^{+/-}$ mice. Similar results were also found in the aged-SAMP8 mice (Fig. 4Q, R). Conversely, in the GSK-3α overexpressed SAMP8 mice, the activation of mTORC1 signaling and the hyperphosphorylation of ULK1 were alleviated (Fig. 4S, T). In addition, we found that neuronal necroptosis was inhibited in the BLA by treating SAMP8 mice with Rapamycin, an inhibitor of mTOR [45] (Supplementary Fig. 14A–C). Together, these findings suggested that the activation of mTORC1 signaling induced autophagy dysfunction participated in the necroptosis in aged mice.

Reduced social interaction accelerates necroptosis in the BLA and impairs behavioral flexibility in 4-month-old SAMP8 mice

Older age is associated with reduced social interactions, extended periods of time living alone, and an increased prevalence of loneliness [46, 47]. Loneliness and social isolation have been shown to promote the cognitive alterations among aged people and animals [48, 49]. Moreover, due to social and demographic changes, increasingly many people are at risk of loneliness in modern society [50], and this risk is further exacerbated in the current context of recurrent or sporadic outbreaks of COVID-19 worldwide. However, it is not clear whether loneliness affects behavioral flexibility in aged animals. We divided the 3-month-old SAMP8 mice into two groups; half of them were housed in separate cages to reduced social interactions (I-SAMP8) and half of them were housed with three other mice to provide social interaction (S-SAMP8) (Fig. 5A). Four weeks later (when the mice were 4 months old), we found that I-SAMP8 mice but not S-SAMP8 mice impaired behavioral flexibility (Fig. 5B–E). The immunostaining with NeuN indicated that the loss of BLA neurons in the I-SAMP8 mice (Fig. 5F, G). Moreover, the levels of RIPK3, pRIPK3, MLKL and pMLKL were significantly increased in the BLA of I-SAMP8 mice when compared with S-SAMP8 mice (Fig. 5H, I). Importantly, the membranous translocation of pMLKL was more apparent in the BLA of I-SAMP8 mice (Fig. 5J, K). Concomitantly, we observed the loss of GSK-3α (Fig. 5H, I, Supplementary Fig. 15A), as well as the activation of mTORC1 signaling (Fig. 5L, M) in the amygdala of I-SAMP8 mice. By injected the AAV-GSK-3α into the BLA of I-SAMP8 mice (Fig. 5N), the impairment of behavioral flexibility in the I-SAMP8 mice were significantly alleviated (Fig. 5O, R). No apparent alteration was found in the OFT task, but I-SAMP8 mice showed a smaller decrease in numbers of entry into the open arm compared to S-SAMP8 mice in EPM task, indicating social isolation increased slightly anxiety-like behavior in mice (Supplementary Fig. 15B–E). In addition, the inhibition of mTORC1 signal by rapamycin administration also rescued behavioral flexibility and alleviated the necroptosis in the social isolated SAMP8 mice (Fig. 5S–U, Supplementary Fig. 16A–C). These data strongly suggested that reduced the social interaction facilitated the necroptosis and impaired behavioral flexibility by the decreasing of GSK-3α regulated the mTOR signal in aged mice.

DISCUSSION

Previous studies reported the impaired behavioral flexibility in the aged rodents [1, 19], while the underlying mechanisms were not clear. In this study, we first demonstrated that the activation of neuronal necroptosis induced BLA neuron loss drive the behavioral inflexibility of aged mice. Using in vivo multiple-electrodes electrophysiological recording and immunohistochemistry, we further revealed that the loss of neurons significantly reduced the activity population in BLA, the critical brain region for behavioral flexibility [6]. In a recent study, necroptosis was found

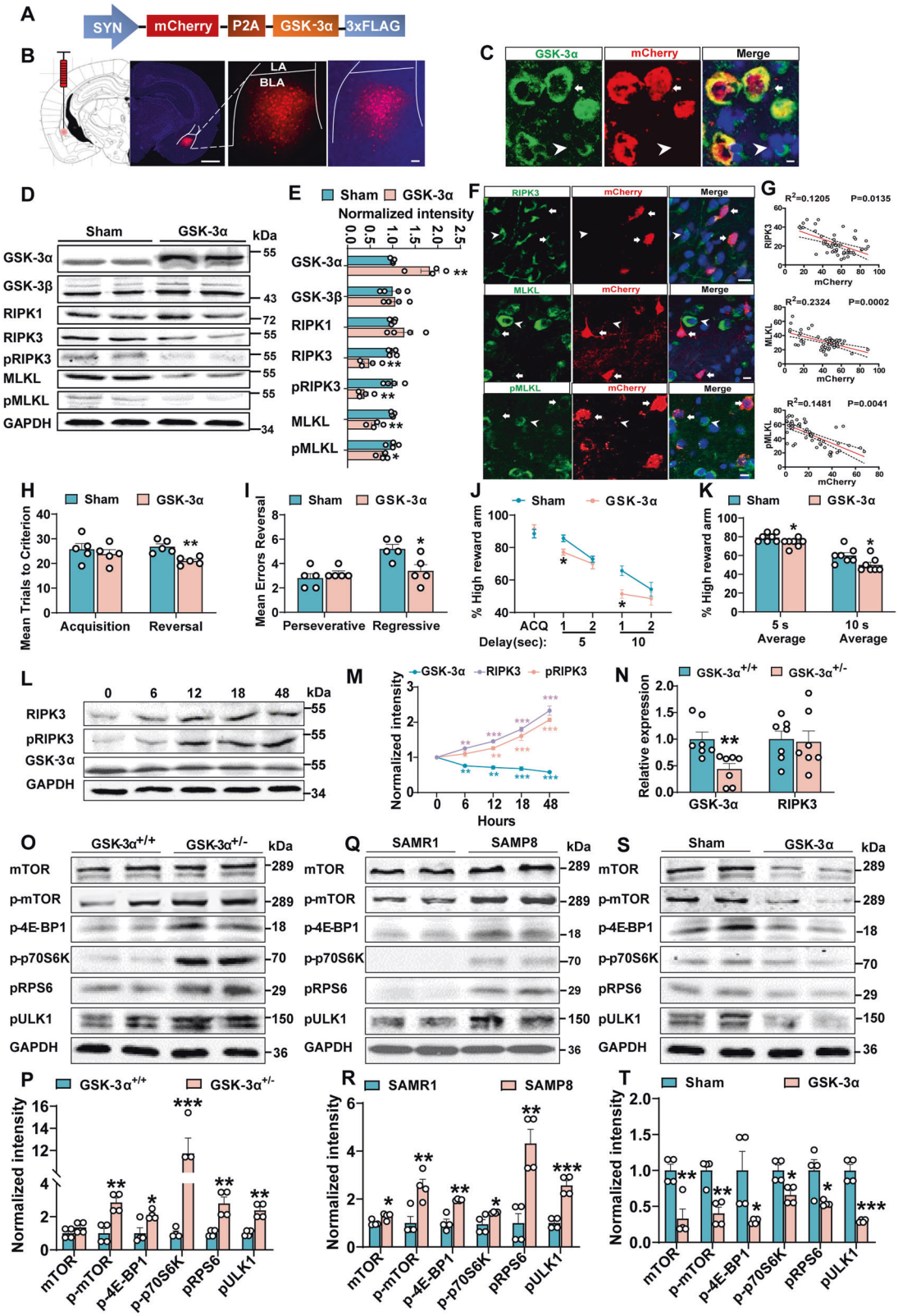

to be activated in AD brains and negatively correlated with cognitive scores [32]. In addition, necroptosis could be found in many neurodegenerative disorders, such as PD and ALS [51]. It was reported that necroptosis could release of damage-associated molecular patterns (DAMPs) and promote inflammation, one of the key features of mammalian aging [52]. These lines of data suggested the critical role of neuronal necroptosis in the pathogenesis of numerous neurological disorders. Consistently, we found that administration of Nec-1s, a specific necroptosis inhibitor, effectively reversed the behavioral inflexibility in

Fig. 4 Restoration of GSK-3α alleviated necroptosis in the BLA and the impairment of behavioral flexibility, and the mTORC1 signaling played an important role in the necroptosis induced by loss of GSK-3α. A Schematic diagram showed the AAV-GSK-3α-mCherry virus construct. **B** Representative fluorescence image showed infection of the virus into the BLA (Bar = 1 mm, left; Bar = 100 μm, right). **C** Amygdala slices from SAMP8 mice infected with AAV-GSK-3α in BLA stained with anti-GSK-3α antibody (Green) (Bar = 5 μm). Arrowheads indicate neurons without virus infection; arrows indicate neurons with virus infection. The protein levels of GSK-3α, GSK-3β, and necroptosis markers from the amygdala of SAMP8 mice treated with AAV-GSK-3α (GSK-3α) and the control virus (Ctrl) were detected by western blotting. The representative images were shown in **D** and the quantitative analysis was shown in **E**. The immunofluorescence images in BLA from the GSK-3α group by using anti-RIPK3, anti-MLKL, anti-pMLKL antibodies (Bar = 10 μm). The representative images were shown in **F** and the correlation analysis was performed (**G**). Arrowheads indicated neurons without virus infected; Arrows indicated neurons with virus infected. The mean number of trials to reach criterion for SAMP8 mice treated with AAV-GSK-3α (GSK-3α) and the control virus group (Sham) during acquisition and reversal (**H**), the mean number of perseverative and regressive errors during reversal between GSK-3α and Sham group (**I**). The percentage of HRA chosen during acquisition test or when the delay time was set at 5 s and 10 s for SAMP8 mice treated with AAV-GSK-3α and the control virus group (**J**), the percentage mean of HRA chosen from GSK-3α and Sham group when the delay time was set at 5 s and 10 s (**K**). The N2a cells were transfected with sh-GSK-3α, and the cell lysates were collected at 0, 6, 12, 18, and 48 h to examine the levels of GSK-3α, RIPK3 and pRIPK3. The representative images were shown in **L** and the quantitative analysis was shown in **M**. **N** The levels of GSK-3α mRNA and RIPK3 mRNA in the amygdala extracts from GSK-3$\alpha^{+/-}$ and GSK-3$\alpha^{+/+}$ mice were examined by RT-PCR. The protein levels of mTOR, p-mTOR (Ser2448), p-4E−BP1 (Thr37/46), p-p70S6K (Thr389), pRPS6 (Ser235/236), pULK1 (Ser757) in the amygdala homogenates from GSK-3$\alpha^{+/-}$ and GSK-3$\alpha^{+/+}$ mice were examined by western blotting. The representative images were shown in **O** and the quantitative analysis was shown in **P**. The protein levels of mTOR, p-mTOR, p-4E−BP1, p-p70S6K, pRPS6, pULK1 in the amygdala tissues of 5-month SAMP8 and age matched SAMR1 mice were detected by western blotting. The representative images were shown in **Q** and the quantitative analysis was shown in **R**. The protein levels of mTOR, p-mTOR, p−4E-BP1, p-p70S6K, pRPS6, pULK1 from the amygdala of SAMP8 mice infected with AAV-GSK-3α virus and the control virus were detected by western blotting. The representative images were shown in **S** and the quantitative analysis was shown in **T**. *$p < 0.05$, **$p < 0.01$, ***$p < 0.001$, vs Sham (for panel **E** and **H**–**K**); *vs* 0 h (for panel **M**); *vs* GSK-3$\alpha^{+/+}$ mice (for panels **N** and **P**); *vs* SAMR1 mice (for panel **R**); *vs* SAMP8 mice injected with control virus (for panel **T**). (Data are represented as mean ± SEM; Multiple *t* test adjusted with Holm-Sidak test, two-way ANOVA with Sidak post hoc comparison test and two-way ANOVA with Dunnett's post hoc test; $n = 4$–7; Cell number = 50–55 for panel **G**).

5-month-old SAMP8 mice. In line with our data, application of Nec-1s, also ameliorated the cognitive impairments in animal models of AD [53], ischemic stroke [54], and prediabetic symptoms [55], as well as the D-galactose-induced mouse model of aging [56]. Suberoylanilide hydroxamic acid (SAHA), a pan-HDAC inhibitor that was able to reverse the memory impairments in AD mice [57], could protect cells from the necroptosis by inhibiting Akt and mTOR signaling pathways [58]. These lines of evidence strongly suggested the critical role of necroptosis in aging and aging-related brain disorders, and inhibition of necroptosis might be a promising approach to hamper those abnormalities.

GSK-3α and GSK-3β are two isoforms of GSK-3, the critical serine/threonine protein kinases that are involved in cell differentiation and death [40]. Evidence has suggested that neuronal GSK-3α contributes more to behavior and cognition than GSK-3β. Neuron-specific deletion of GSK-3α induced significant impairments in learning and working memory [59]. GSK-3α mutant mice displayed multiple behavioral abnormalities, including increased grooming activity, decreased exploratory activity, reduced aggressive behavior, decreased social motivation, and associative memory [60]. These findings revealed the irreplaceable role of GSK-3α in physiological brain function. In our study, we first identified that the loss of GSK-3α led to behavioral inflexibility in aged mice. Namely, the loss of GSK-3α resulted in cognitive changes in aging. In line with our findings, acceleration of aging-related pathologies, including severe vacuolar degeneration of myofibrils, and premature senescence in hepatocytes, could be found in global GSK-3α KO mice [42]. This evidence strongly suggests a key role for GSK-3α in aging-related degeneration or abnormalities.

We further studied how GSK-3α loss contributed to necroptosis in the BLA. Previous studies had revealed a critical role of GSK-3α in mediating neuronal death when neurons underwent various insults [61–63]. Here, we found that the loss of GSK-3α promoted RIPK1-independent necroptosis. This was consistent with a previous report about the role of GSK-3α inhibition in regulating drug-resistance and chemotherapy-induced necroptosis [64]. We further explored how GSK-3α inhibition could initiate the necroptosis by RIPK3 and found that the degradation but not the transcription of RIPK3 was impaired. It is known that the mTORC1 signaling pathway play an important role in mediating the degradation of RIPK3 *via* autophagy and the abnormally activation of the mTORC1 signaling can be found in aged mice [42], or upon the inhibition of GSK-3 [65–67]. Here, we found that genetic deletion of GSK-3α in BLA activated mTORC1 signaling, which, in turn, resulted in the dysfunction of autophagy and RIPK3 accumulation. Overexpression of GSK-3α in BLA tempered the activation of mTORC1 signaling and reduced the RIPK3 levels. Importantly, the activation of mTOR signaling has been demonstrated to drive multiple dysfunctions, including cerebrovascular, synapse, and cognitive impairment in normative normal aging [68]. In addition, the activity of mTORC1 can be regulated via phosphorylation by the repressor TSC1/TSC2 complexes, which were negatively regulated by GSK-3 [69]. Thus, the activation of mTORC1 signaling due to the inhibition of GSK-3α in aging might be a key modulator of aging-related disorders.

In our study, we finally identified that social isolation could accelerate behavioral inflexibility in SAMP8 mice. It is known that the decline of social activities in the elderly leads to social isolation, which, in turn, increases the risk of loneliness [49]. Under normal circumstances, the elderly is at higher risk of social isolation compared with younger person [70], this concern has been exacerbated in the current COVID-19 pandemic [71]. Physical distancing restrictions and stay-at-home orders to prevent the spread of SARS-CoV-2 virus increase the risk of social isolation and loneliness for the elderly, especially for those who are not good at using online information communication [71]. Research has linked social isolation and loneliness to higher risks for a variety of physical and mental conditions: high blood pressure, heart disease, obesity, a weakened immune system, anxiety, depression, cognition decline, AD, and even death [72–75]. Some studies that examined the quantitative parameters of social isolation (e.g., number and frequency) revealed the tight correlation of social isolation or low levels of social contact with different dimensions of cognition, especially cognitive decline and dementia in aged people [76]. Consistent with our findings, Li and Powell reported that isolation rearing impaired behavioral flexibility in rats [77, 78]. In contrast, participation in some forms of social activity, such as senior citizen clubs or frequent contact with offspring reduced the cognitive decline in older adults [79]. Here, we found that social isolation promoted necroptosis in the BLA of aged mice. Accordingly, social isolation had been suggested to promote

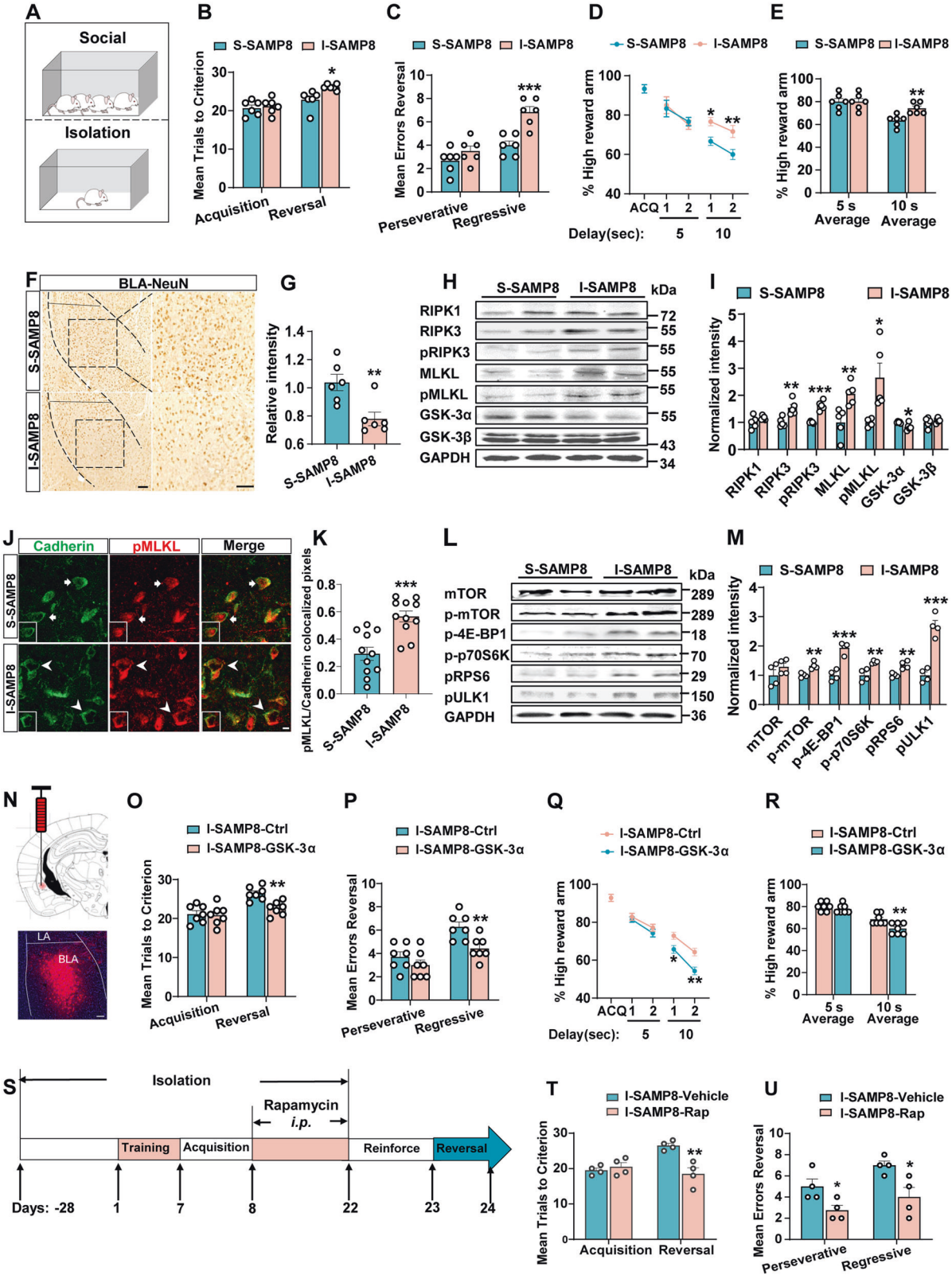

hippocampal cell death and the inflammatory response after cardiac arrest [80]. In contrast, enhanced social interaction could ameliorate neuronal loss following closed head injury in mice [81]. Collectively, these lines of evidence strongly suggest the importance of social activity for cognitive function, indicating a phenomenon in which social isolation accelerates the inability for older adults to adapt to the diverse circumstances. This phenomenon is especially noteworthy given its relevance to present conditions, such as COVID-19, and the measures taken to prevent its spread.

Fig. 5 Social isolation accelerated the necroptosis in the BLA and the dysfunction of behavioral flexibility in 4-month-SAMP8 mice. **A** Diagram for the social isolated (I-SAMP8) or group-housed (S-SAMP8) SAMP8 mice. The mean number of trials to reach criterion for S-SAMP8 and I-SAMP8 group during acquisition and reversal **(B)**, the mean number of perseverative and regressive errors during reversal for S-SAMP8 and I-SAMP8 group **(C)**. The percentage of HRA chosen during acquisition test or when the delay time was set at 5 s and 10 s for S-SAMP8 and I-SAMP8 group **(D)**, the percentage mean of HRA chosen from S-SAMP8 and I-SAMP8 group when the delay time was set at 5 s and 10 s **(E)**. The coronal slices from S-SAMP8 and I-SAMP8 mice were stained with anti-NeuN antibody. The representative images were shown in **F** (Bar = 100 μm), and the relative intensity analysis was shown in **G**. Representative immunoblots with anti-GSK-3α, anti-GSK-3β, and necroptosis markers from S-SAMP8 and I-SAMP8 group mice **(H)** and quantitative analysis was performed in **I**. The coronal slices from S-SAMP8 and I-SAMP8 mice were stained with anti-Cadherin (Green) and anti-pMLKL (Red) antibodies. The representative images were shown in **J** (Bar = 5 μm) and the colocalization efficiency of cadherin and pMLKL was analyzed in **K**. Arrows indicated cell without membranous translocation of pMLKL; Arrowheads indicated cell with membranous translocation of pMLKL. The protein levels of mTOR, p-mTOR, p-4E-BP1, p-p70S6K, pRPS6, pULK1 from the amygdala of S-SAMP8 and I-SAMP8 mice were detected by western blotting. The representative images were shown in **L** and the quantitative analysis was shown in **M**. **N** The representative virus infection image in the BLA of I-SAMP8 mice. (Bar = 100 μm). The mean number of trials to reach criterion for I-SAMP8 mice infected with AAV-GSK-3α virus (I-SAMP8-GSK-3α) and the control virus (I-SAMP8-Ctrl) during acquisition and reversal **(O)**, the mean number of perseverative and regressive errors during reversal for I-SAMP8-Ctrl and I-SAMP8-GSK-3α group **(P)**. The percentage of HRA chosen during acquisition test or when the delay time was set at 5 s and 10 s for I-SAMP8-Ctrl and I-SAMP8-GSK-3α group **(Q)**, the percentage mean of HRA chosen from I-SAMP8-Ctrl and I-SAMP8-GSK-3α group when the delay time was set at 5 s and 10 s **(R)**. **S** Timeline of the rapamycin injection and the experimental procedures for reversal learning. The mean number of trials to reach criterion for I-SAMP8 mice injected with rapamycin (I-SAMP8-Rap) and the vehicle (I-SAMP8-Vehicle) during acquisition and reversal **(T)**, the mean number of perseverative and regressive errors during reversal for I-SAMP8-Vehicle and I-SAMP8-Rap group **(U)**. *$p < 0.05$, **$p < 0.01$, ***$p < 0.001$, *vs* S-SAMP8 (for panels **B**–**M**) or I-SAMP8-Ctrl (for panel **O**–**R**) or I-SAMP8-Vehicle (for panels **T**–**U**) (Data are represented as mean ± SEM; Unpaired *t*-test; Multiple *t*-test adjusted with Holm-Sidak and two-way ANOVA with Sidak post hoc comparison test; $n = 4$–11).

Taken together, our findings here revealed a critical role of GSK-3α loss in the aging-related necroptosis in the BLA, which, in turn, leads to behavioral inflexibility, a higher level of cognitive impairment. In addition, we also demonstrated that social isolation is a risk factor for the elderly to adjust adaptive behavior in response to changing environment (Supplementary Fig. 17).

MATERIALS AND METHODS

Animals and brain of cynomolgus monkeys

SAMP8 and SAMR1 mice were purchased from the Department of Laboratory Animal Science, Peking University Health Science Center. GSK-3α$^{flox/+}$ mice were kindly gift from Dr. James R Woodgett [82]. The amygdala tissues of 8-year-old and 25-year-old cynomolgus monkeys were acquired from Guangdong Key Laboratory of Non-human Primate Research. Genotyping for GSK-3α$^{flox/+}$ mice were performed by multiplex PCR using a pair of forward (5′-cccccaccaagtgatttcactgcta-3′) and reverse (5′- cttgaacctttttgtcctgaagaacc-3′) primers. All mice used in this study were male mice with C57BL/6 background. All animal experiments were carried out according to the "Policies on the Use of Animals and Humans in Neuroscience Research" revised by the Society for Neuroscience in 1995 and approved by the animal ethnic committee of Tongji Medical College, Huazhong University of Science and Technology.

Odor-based reversal learning

Apparatus. Animals were trained in an open field arena (40 × 40 × 30 cm^3) with two bowls filled with sand and Froot Loops buried in each bowl (8 cm diameter × 2 cm high). The bowls were kept 15 cm apart.

Behavioral training. All animals were food restricted to maintain at approximately 85% of their initial free-feeding weight, and fetched water anytime. On the first day of habituation, two 1/2 pieces of Froot Loops cereal (Kellogg, Thailand) were placed on top of the sand. Animals were placed in the middle of two bowls and allowed to navigate and consume the cereal pieces. After animals consumed all the cereal pieces, the animals returned to their home cage. The sand bowls were baited again and the mouse was sent back to the home cage. On the second habituation day, the procedure was the same as on Day 1. On subsequent days, only half a piece of cereal was placed in each bowl. The pieces were submerged in the sand until no longer visible and animals had to dig in the sand to obtain the cereal piece. This procedure was terminated when animals retrieved cereal pieces that were completely buried for two consecutive days. During discrimination and reversal testing, odor pairs were randomly used and paired as rewarded and unrewarded odors. Suprathreshold olfactory stimuli consisted of powdered odorants (curry, cinnamon and garlic) mixed in two bowls filled with sand. During the acquisition stage, animals were trained to discriminate between rewarded and unrewarded odor. The location of the rewarded odor was randomly switched between two adjacent locations (with no more than three repetitions for a single location). An intertrial interval of 15 s was used. Testing was conducted in two phases: acquisition and reversal. Acquisition was terminated when animals made 9/10 consecutive correct choices in a moving block of 10 trials. On the second day, animals were trained in the same way, except that the rewarded odor from the previous day was unrewarded and the previously unrewarded odor was rewarded. Errors were divided into *perseverative and regressive* types. *Perseveration* was defined as selecting the unrewarded odor for three or more trials in a block of four consecutive trials. Once animals made fewer than three errors in a four trial block, the subsequent errors were no longer counted as perseverative errors. Since then, the number of errors was counted as *regressive errors*. The criterion and methods were used and described in previous studies [83].

Delay-based flexible decision-making

Apparatus. Experiments were conducted in an elevated, high-sided T-maze. The T-maze consisted of three arms: a start arm and two perpendicular reward arms (Fig. 1E). The sizes of the arms are as follows: each reward arm, 26.5 × 8 × 18 cm (L × W × H); start arm, 36 × 8 × 18 cm. A raised food well was placed 2 cm from the back wall of each reward arm. In addition, each reward arms contained two 20-cm-high, 7.5-cm-wide gates, placed 1 cm from the entrance and 5 cm from the end wall, which could be opened or closed to control the entry and exit of mice to and from the arms and food wells.

Procedure. Stage 1: Habituation

During the experiment procedure, all animals were fed a restricted diet and maintained at approximately 85% of their initial free-feeding weight. Animals had access to water at all time. For the first two days, mice were placed in the start arm of the maze and allowed to explore the T-maze for 5 min One food pellet (14 mg, Bio-Serv, USA) was placed in the food well of each reward arm. For the next two days, animals were again placed in the start arm and allowed to investigate the T-maze, but in this stage, five food pellets were placed in each food well [37]. All the gates were open during the habituation.

Stage 2: Discrimination of the HRA from the low-reward arm (LRA)

Forced arm entry phase: In this phase, one of the reward arms was selected as the HRA, and the other was selected as the LRA. In order to avoid position preference, each group of animals was divided into two subgroups. The positions of the HRA and LRA in these two subgroups were opposite. Over a period of 2 days, animals completed ten trials per day. Five reward pellets were available in the HRA, but only one was available in the LRA [84]. During this phase, when the mouse entered one reward arm, it was confined in this arm to eat the pellets (up to 60 s). Then, the mice were liberated to the starting arm. Ten seconds later, the start door was opened, and a new trial began.

Free arm entry phase: In this phase, the mice completed 10 trials per day. In the beginning, gates A and D were closed. When the mice entered the LRA (HRA), gate A (D) was open, and gate C (B) was closed immediately. After the mice ate all the reward pellets in the chosen arm, they returned to the starting arm for the next trial. Training will be ended up until the mice hold the selection probability of HRA for over 80% of total trials for two consecutive days. Mice were excluded if they could not meet the above criteria.

Stage 3: Testing stage

During this stage, the protocol was applied according to the free arm entry phase in stage 2. When the mice entered the HRA, gate C was closed immediately, while gate D was opened after delays of 5 s and 10 s to test the delay-based flexible decision-making.

Electrophysiology

The electrophysiology experiment was performed as described previously [85, 86]. Mice were anesthetized with isoflurane (1% to 3%) and were placed in a stereotaxic frame (Newdoon) with the head fixed and were implanted unilaterally four tetrodes made of twisted 17 μm Formvar-coated platinum-iridium wires (California Fine Wire Company) in the BLA (AP: − 1.3 mm; ML: ± 3.4 mm; DV: 4.8–4.9 mm). All implants were fixed with stainless steel screws and dental cement. A stainless steel screw also served as ground electrode through sliver wires. After mice recovered from the surgery for at least 1 week, electrodes were connected to AC-coupled unity-gain operational amplifiers (Plexon). Recording was then performed from pre-learning (home cage), learning, and learnt stages during reversal learning. The electrical signal was amplified 4000- to 8000-fold, filtered at 0.05 Hz–8 kHz, down-sampled to a rate of 1000 Hz, and low-pass filtered at 250 Hz for local field potential recording. After electrophysiological recordings, the mouse brains were sliced to verify electrode placement. Analysis of the LFP signal was performed in MATLAB.

Stereotaxic injection and drug treatment

For stereotaxic injection, mice were anesthetized with ketamine (100 mg/kg) and dexmedetomidine (0.5 mg/kg), and then the head was fixed in the stereotaxic apparatus (RWD life science, China). The scalp was sterilized with iodophors, holes were drilled bilaterally and a total of 0.3 μl virus were microinfused into the amygdala *via* an automatic microinjection system (Reno, NV, USA). The virus was injected into both side of the amygdala of SAMP8 mice (AP:−1.4 mm; ML:±3.4 mm; DV:−4.9 mm), GSK-3α $^{flox/+}$ and C57BL/6 mice (AP:−1.3 mm; ML:±3.4 mm; DV:−4.86 mm). The infusion rate was 0.03 μL/min. The AAV2/8-hSyn-GSK-3α and AAV2/8- hSyn-Cre viruses were purchased from Obio Technology (Shanghai, China). AAV9-hSyn-Bmp15 viruses were purchased from Brain Case (Shenzhen, China). The lentivirus packaged sh-GSK3α and the scrambled control were purchased from Genechem (Shanghai, China). The valid target sequence of sh-GSK3α is ACCCATCCTCACAAGCTTTAA. The lentivirus packaged sh-GSK3β and the scrambled control were purchased from Obio Technology (Shanghai, China). The valid target sequence of sh-GSK3β is CCACAGAACCTCTTGTTG GAT. Animals were used for detection 4 weeks post the injection. We assigned mice to different groups according to their species and injected virus. For different groups of the same species, we randomly assigned before injecting different viruses. For drug treatment, the necroptosis inhibitor, 7-Cl-O-Nec-1 (Nec-1s, Millpore, 504297) and vehicle (DMSO 1%, methylbeta-cyclodextrin 4% in PBS) were injected intraperitoneally at a dose of 10 mg/kg for one week before behavior training, maintaining the same dose during behavior training and testing. The inhibitor of mTOR signaling, rapamycin (Abmole, M1768), and vehicle (0.2% CMC and 0.25% Tween-80 in ddH_2O) were injected intraperitoneally at a dose of 2.5 mg/kg once daily for two weeks.

Microarray

The amygdala tissues were isolated from SAMR1 and SAMP8 mice and tissues were homogenized using a TissueRuptor (Qiagen, Palo Alto, CA, USA) homogenizer (50/60 Hz) according to the manufacturer's protocol. Total RNA was extracted and treated with an RNase-free DNase (Qiagen, Palo Alto, CA, USA). The RNA concentration was measured by spectrophotometer (DU-640, Beckman, USA), and the RNA integrity was detected by 1% agarose gel electrophoresis. Mouse OneArray (Phalanx Biotech Group, Hsinchu, China) v2 (MOA-002) chips with 26,423 mouse genome probes and 872 experimental control probes were used to analyze gene expression profile.

Statistical analysis

All data are shown as means ± SEM and analyzed using unpaired *t*-test, multiple *t*-test adjusted with Holm-Sidak, one-way ANOVA with Tukey's post hoc comparison, two-way ANOVA with Dunnett's post hoc comparison, two-way ANOVA with Tukey's post hoc comparison and two-way ANOVA with Sidak post hoc comparison. All the statistical analyses were done using GraphPad Prism 8.0 software. Sample sizes were estimated on the basis of the previous studies [87]. Detail methods of statistical analyses was showed in the Supplementary Table 3.

REFERENCES

1. Breton YA, Seeland KD, Redish AD. Aging impairs deliberation and behavioral flexibility in inter-temporal choice. Front Aging Neurosci. 2015;7:41.
2. Diamond A, Lee K. Interventions shown to aid executive function development in children 4 to 12 years old. Science. 2011;333:959–64.
3. Burt KB, Paysnick AA. Resilience in the transition to adulthood. Dev Psychopathol. 2012;24:493–505.
4. Burke SN, Mormino EC, Rogalski EJ, Kawas CH, Willis RJ, Park DC. What are the later life contributions to reserve, resilience, and compensation? Neurobiol Aging. 2019;83:140–4.
5. Uddin LQ. Cognitive and behavioural flexibility: neural mechanisms and clinical considerations. Nat Rev Neurosci. 2021;22:167–79.
6. Calu DJ, Roesch MR, Stalnaker TA, Schoenbaum G. Associative encoding in posterior piriform cortex during odor discrimination and reversal learning. Cereb Cortex. 2007;17:1342–9.
7. Majak K, Ronkko S, Kemppainen S, Pitkanen A. Projections from the amygdaloid complex to the piriform cortex: A PHA-L study in the rat. J Comp Neurol. 2004;476:414–28.
8. Izquierdo A, Murray EA. Combined unilateral lesions of the amygdala and orbital prefrontal cortex impair affective processing in rhesus monkeys. J Neurophysiol. 2004;91:2023–39.
9. Coutureau E, Marchand AR, Di Scala G. Goal-directed responding is sensitive to lesions to the prelimbic cortex or basolateral nucleus of the amygdala but not to their disconnection. Behav Neurosci. 2009;123:443–8.
10. Burgos-Robles A, Kimchi EY, Izadmehr EM, Porzenheim MJ, Ramos-Guasp WA, Nieh EH, et al. Amygdala inputs to prefrontal cortex guide behavior amid conflicting cues of reward and punishment. Nat Neurosci. 2017;20:824.
11. Zeeb FD, Floresco SB, Winstanley CA. Contributions of the orbitofrontal cortex to impulsive choice: interactions with basal levels of impulsivity, dopamine signalling, and reward-related cues. Psychopharmacology. 2010;211:87–98.
12. Roesch MR, Esber GR, Bryden DW, Cerri DH, Haney ZR, Schoenbaum G. Normal aging alters learning and attention-related teaching signals in basolateral amygdala. J Neurosci. 2012;32:13137–44.
13. Mobini S, Body S, Ho MY, Bradshaw CM, Szabadi E, Deakin JF, et al. Effects of lesions of the orbitofrontal cortex on sensitivity to delayed and probabilistic reinforcement. Psychopharmacol (Berl). 2002;160:290–8.
14. Winstanley CA, Eagle DM, Robbins TW. Behavioral models of impulsivity in relation to ADHD: Translation between clinical and preclinical studies. Clin Psychol Rev. 2006;26:379–95.
15. Tait DS, Chase EA, Brown VJ. Tacrine improves reversal learning in older rats. Neuropharmacology. 2013;73:284–9.
16. Uprety A, Moss MB, Rosene DL, Killiany RJ, Moore TL, Curcumin improves reversal learning in middle-aged rhesus monkeys. Behav Neurosci. 2022;136:126–38.
17. Schoenbaum G, Nugent S, Saddoris MP, Gallagher M. Teaching old rats new tricks: Age-related impairments in olfactory reversal learning. Neurobiol Aging. 2002;23:555–64.
18. Eppinger B, Schuck NW, Nystrom LE, Cohen JD. Reduced striatal responses to reward prediction errors in older compared with younger adults. J Neurosci. 2013;33:9905–12.
19. Simon NW, LaSarge CL, Montgomery KS, Williams MT, Mendez IA, Setlow B, et al. Good things come to those who wait: Attenuated discounting of delayed rewards in aged Fischer 344 rats. Neurobiol Aging. 2010;31:853–62.
20. Morrison JH, Hof PR. Life and death of neurons in the aging brain. Science. 1997;278:412–9.
21. Haug H, Kuhl S, Mecke E, Sass NL, Wasner K. The significance of morphometric procedures in the investigation of age changes in cytoarchitectonic structures of human brain. J Hirnforsch. 1984;25:353–74.
22. West MJ. Regionally specific loss of neurons in the aging human hippocampus. Neurobiol Aging. 1993;14:287–93.
23. Kordower JH, Chu Y, Stebbins GT, DeKosky ST, Cochran EJ, Bennett D, et al. Loss and atrophy of layer II entorhinal cortex neurons in elderly people with mild cognitive impairment. Ann Neurol. 2001;49:202–13.

24. Li GM, Cheng HY, Zhang XZ, Shang XM, Xie H, Zhang X, et al. Hippocampal neuron loss is correlated with cognitive deficits in SAMP8 mice. Neurol Sci. 2013;34:963–9.
25. Niikura T, Tajima H, Kita Y. Neuronal cell death in Alzheimer's disease and a neuroprotective factor, humanin. Curr Neuropharmacol. 2006;4:139–47.
26. Aisen PS, Petersen RC, Donohue M, Weiner MW, Alzheimer's Disease Neuroimaging I. Alzheimer's disease neuroimaging initiative 2 clinical core: progress and plans. Alzheimers Dement. 2015;11:734–9.
27. Lalaoui N, Lindqvist LM, Sandow JJ, Ekert PG. The molecular relationships between apoptosis, autophagy and necroptosis. Semin Cell Dev Biol. 2015;39:63–69.
28. Arguelles S, Guerrero-Castilla A, Cano M, Munoz MF, Ayala A. Advantages and disadvantages of apoptosis in the aging process. Ann NY Acad Sci. 2019;1443:20–33.
29. Deepa SS, Unnikrishnan A, Matyi S, Hadad N, Richardson A, Necroptosis increases with age and is reduced by dietary restriction. Aging Cell. 2018;17:e12770.
30. Murakami Y, Matsumoto H, Roh M, Giani A, Kataoka K, Morizane Y, et al. Programmed necrosis, not apoptosis, is a key mediator of cell loss and DAMP-mediated inflammation in dsRNA-induced retinal degeneration. Cell Death Differ. 2014;21:270–7.
31. Meng LJ, Jin W, Wang XD. RIP3-mediated necrotic cell death accelerates systematic inflammation and mortality. P Natl Acad Sci USA. 2015;112:11007–12.
32. Caccamo A, Branca C, Piras IS, Ferreira E, Huentelman MJ, Liang WS, et al. Necroptosis activation in Alzheimer's disease. Nat Neurosci. 2017;20:1236.
33. Re DB, Le Verche V, Yu CH, Amoroso MW, Politi KA, Phani S, et al. Necroptosis drives motor neuron death in models of both sporadic and familial ALS. Neuron. 2014;81:1001–8.
34. Iannielli A, Bido S, Folladori L, Segnali A, Cancellieri C, Maresca A, et al. Pharmacological inhibition of necroptosis protects from dopaminergic neuronal cell death in Parkinson's disease models. Cell Rep. 2018;22:2066–79.
35. Amson R, Lassalle JM, Halley H, Prieur S, Lethrosne F, Roperch JP, et al. Behavioral alterations associated with apoptosis and down-regulation of presenilin 1 in the brains of p53-deficient mice. Proc Natl Acad Sci USA. 2000;97:5346–50.
36. Yanai S, Endo S. Early onset of behavioral alterations in senescence-accelerated mouse prone 8 (SAMP8). Behav Brain Res. 2016;308:187–95.
37. Rudebeck PH, Walton ME, Smyth AN, Bannerman DM, Rushworth MF. Separate neural pathways process different decision costs. Nat Neurosci. 2006;9:1161–8.
38. Abela AR, Duan YR, Chudasama Y. Hippocampal interplay with the nucleus accumbens iscritical for decisions about time. Eur J Neurosci. 2015;42:2224–33.
39. Hernandez CM, Orsini CA, Labiste CC, Wheeler AR, Ten Eyck TW, Bruner MM, et al. Optogenetic dissection of basolateral amygdala contributions to intertemporal choice in young and aged rats. Elife 2019;8:e46174.
40. Cohen P, Frame S. The renaissance of GSK3. Nat Rev Mol Cell Biol. 2001;2:769–76.
41. Zhou J, Freeman TA, Ahmad F, Shang X, Mangano E, Gao E, et al. GSK-3alpha is a central regulator of age-related pathologies in mice. J Clin Invest. 2013;123:1821–32.
42. Zhou JB, Freeman TA, Ahmad F, Shang XY, Mangano E, Gao EH, et al. GSK-3 alpha is a central regulator of age-related pathologies in mice. J Clin Invest. 2013;123:1821–32.
43. Ahmad F, Lal H, Zhou JB, Vagnozzi RJ, Yu JE, Shang XY, et al. Cardiomyocyte-specific deletion of Gsk3 alpha mitigates post-myocardial infarction remodeling, contractile dysfunction, and heart failure. J Am Coll Cardiol. 2014;64:696–706.
44. Xie YD, Zhao YF, Shi L, Li W, Chen K, Li M, et al. Gut epithelial TSC1/mTOR controls RIPK3-dependent necroptosis in intestinal inflammation and cancer. J Clin Invest. 2020;130:2111–28.
45. Blagosklonny MV. Rapamycin for longevity: opinion article. Aging. 2019;11:8048–67.
46. Hansen T, Slagsvold B. Late-life loneliness in 11 European countries: results from the generations and gender survey. Soc Indic Res. 2016;129:445–64.
47. Rico-Uribe LA, Caballero FF, Olaya B, Tobiasz-Adamczyk B, Koskinen S, Leonardi M, et al. Loneliness, social networks, and health: a cross-sectional study in three countries. PLoS One 2016;11:e0145264.
48. Chen YRR, Schulz PJ, The effect of information communication technology interventions on reducing social isolation in the elderly: a systematic review. J Med Internet Res. 2016;18:e18.
49. Cacioppo JT, Hawkey LC. Perceived social isolation and cognition. Trends Cogn Sci. 2009;13:447–54.
50. Masi CM, Chen HY, Hawkley LC, Cacioppo JT. A meta-analysis of interventions to reduce loneliness. Pers Soc Psychol Rev. 2011;15:219–66.
51. Shao LF, Yu SP, Ji W, Li HZ, Gao YL. The contribution of necroptosis in neurodegenerative diseases. Neurochem Res. 2017;42:2117–26.
52. Royce GH, Brown-Borg HM, Deepa SS. The potential role of necroptosis in inflammaging and aging. Geroscience. 2019;41:795–811.
53. Yang SH, Lee DK, Shin J, Lee S, Baek S, Kim J, et al. Nec-1 alleviates cognitive impairment with reduction of A and tau abnormalities in APP/PS1 mice. Embo Mol Med. 2017;9:61–77.
54. Zhang S, Wang Y, Li D, Wu J, Si W, Wu Y, Necrostatin-1 attenuates inflammatory response and improves cognitive function in chronic ischemic stroke mice. Medicines 2016; 3.
55. Jinawong K, Apaijai N, Wongsuchai S, Pratchayasakul W, Chattipakorn N, Chattipakorn SC. Necrostatin-1 Mitigates Cognitive Dysfunction in Prediabetic Rats With No Alteration in Insulin Sensitivity. Diabetes. 2020;69:1411–23.
56. Duan SC, Wang XQ, Chen G, Quan CX, Qu SQ, Tong JB, Inhibiting RIPK1 limits neuroinflammation and alleviates postoperative cognitive impairments in d-galactose-induced aged mice. Front Behav Neurosci. 2018;12:138.
57. Benito E, Urbanke H, Ramachandran B, Barth J, Halder R, Awasthi A, et al. HDAC inhibitor-dependent transcriptome and memory reinstatement in cognitive decline models. J Clin Invest. 2015;125:3572–84.
58. Wang D, Zhao M, Chen GZ, Cheng X, Han XX, Lin S, et al. The histone deacetylase inhibitor vorinostat prevents TNF alpha-induced necroptosis by regulating multiple signaling pathways. Apoptosis. 2013;18:1348–62.
59. Maurin H, Lechat B, Dewachter I, Ris L, Louis JV, Borghgraef P, et al. Neurological characterization of mice deficient in GSK3 alpha highlight pleiotropic physiological functions in cognition and pathological activity as Tau kinase. Mol Brain. 2013; 6.
60. Kaidanovich-Beilin O, Lipina TV, Takao K, van Eede M, Hattori S, Laliberte C, et al. Abnormalities in brain structure and behavior in GSK-3alpha mutant mice. Mol Brain. 2009; 2.
61. Russell JC, Kishimoto K, O'Driscoll C, Hossain MA. Neuronal pentraxin 1 induction in hypoxic-ischemic neuronal death is regulated via a glycogen synthase kinase-3 alpha/beta dependent mechanism. Cell Signal. 2011;23:673–82.
62. Nonaka S, Chuang DM. Neuroprotective effects of chronic lithium on focal cerebral ischemia in rats. Neuroreport. 1998;9:2081–4.
63. Nonaka S, Hough CJ, Chuang DM. Chronic lithium treatment robustly protects neurons in the central nervous system against excitotoxicity by inhibiting N-methyl-D-aspartate receptor-mediated calcium influx. Proc Natl Acad Sci USA. 1998;95:2642–7.
64. Grassilli E, Ianzano L, Bonomo S, Missaglia C, Cerrito MG, Giovannoni R, et al. GSK3A is redundant with GSK3B in modulating drug resistance and chemotherapy-induced necroptosis. PLoS One. 2014;9:e100947.
65. Kim YC, Guan KL. mTOR: a pharmacologic target for autophagy regulation. J Clin Invest. 2015;125:25–32.
66. Ha S, Ryu HY, Chung KM, Baek SH, Kim EK, Yu SW, Regulation of autophagic cell death by glycogen synthase kinase-3 beta in adult hippocampal neural stem cells following insulin withdrawal. Mol Brain. 2015; 8:30.
67. Yang Y, Jia YM, Sun QW, Dong HB, Zhao RQ. White light emitting diode induces autophagy in hippocampal neuron cells through GSK-3-mediated GR and ROR alpha pathways. Aging-Us. 2019;11:1832–49.
68. Van Skike CE, Lin AL, Burbank RR, Halloran JJ, Hernandez SF, Cuvillier J, et al. mTOR drives cerebrovascular, synaptic, and cognitive dysfunction in normative aging. Aging Cell 2020;19:e13057.
69. Manning BD, Tee AR, Logsdon MN, Blenis J, Cantley LC. Identification of the tuberous sclerosis complex-2 tumor suppressor gene product tuberin as a target of the phosphoinositide 3-Kinase/Akt pathway. Mol Cell. 2002;10:151–62.
70. Courtin E, Knapp M. Social isolation, loneliness and health in old age: a scoping review. Health Soc Care Comm. 2017;25:799–812.
71. Gorenko JA, Moran C, Flynn M, Dobson K, Konnert C. Social isolation and psychological distress among older adults related to COVID-19: a narrative review of remotely-delivered interventions and recommendations. J Appl Gerontol. 2021;40:3–13.
72. Fratiglioni L, Paillard-Borg S, Winblad B. An active and socially integrated lifestyle in late life might protect against dementia. Lancet Neurol. 2004;3:343–53.
73. Wilson RS, Krueger KR, Arnold SE, Schneider JA, Kelly JF, Barnes LL, et al. Loneliness and risk of Alzheimer disease. Arch Gen Psychiat. 2007;64:234–40.
74. Cacioppo JT, Hawkley LC, Ernst JM, Burleson M, Berntson GG, Nouriani B, et al. Loneliness within a nomological net: An evolutionary perspective. J Res Pers. 2006;40:1054–85.
75. Umberson D, Montez JK. Social relationships and health: a flashpoint for health policy. J Health Soc Behav. 2010;51:S54–66.
76. Read S, Comas-Herrera A, Grundy E. Social isolation and memory decline in later-life. J Gerontol B Psychol Sci Soc Sci. 2020;75:367–76.
77. Amitai N, Young JW, Higa K, Sharp RF, Geyer MA, Powell SB. Isolation rearing effects on probabilistic learning and cognitive flexibility in rats. Cogn Affect Behav Ne. 2014;14:388–406.
78. Li N, Wu X, Li L. Chronic administration of clozapine alleviates reversal-learning impairment in isolation-reared rats. Behav Pharm. 2007;18:135–45.
79. Lee SH, Kim YB, Which type of social activities may reduce cognitive decline in the elderly?: A longitudinal population-based study. BMC Geriatr. 2016;16:165.
80. Weil ZM, Norman GJ, Barker JM, Su AJ, Nelson RJ, DeVries AC. Social isolation potentiates cell death and inflammatory responses after global ischemia. Mol Psychiatr. 2008;13:913–5.

81. Doulames VM, Vilcans M, Lee S, Shea TB, Social interaction attenuates the extent of secondary neuronal damage following closed head injury in mice. Front Behav Neurosci. 2015;9:275.
82. Ahmad F, Lal H, Zhou J, Vagnozzi RJ, Yu JE, Shang X, et al. Cardiomyocyte-specific deletion of Gsk3alpha mitigates post-myocardial infarction remodeling, contractile dysfunction, and heart failure. J Am Coll Cardiol. 2014;64:696–706.
83. Kim J, Ragozzino ME. The involvement of the orbitofrontal cortex in learning under changing task contingencies. Neurobiol Learn Mem. 2005;83:125–33.
84. Zhang Q, Kobayashi Y, Goto H, Itohara, An Automated T-maze based apparatus and protocol for analyzing delay- and effort-based decision making in free moving rodents. J Vis Exp. 2018;57895.
85. Du H, Deng W, Aimone JB, Ge M, Parylak S, Walch K, et al. Dopaminergic inputs in the dentate gyrus direct the choice of memory encoding. Proc Natl Acad Sci USA. 2016;113:E5501–5510.
86. Jing W, Zhang T, Liu J, Huang X, Yu Q, Yu H, et al. A circuit of COCH neurons encodes social-stress-induced anxiety via MTF1 activation of Cacna1h. Cell Rep. 2021;37:110177.
87. Yang X, Yao C, Tian T, Li X, Yan H, Wu J, et al. A novel mechanism of memory loss in Alzheimer's disease mice via the degeneration of entorhinal-CA1 synapses. Mol Psychiatry. 2018;23:199–210.

ACKNOWLEDGEMENTS

We thank Dr. James Woodgett for gifting us the GSK-3α-floxed mice. We thank Dr. Yun -Yun Han at Dept. Neurobiology of HUST and Dr. Keqiang Ye at Shenzhen Institutes of Advanced Technology for their constructive comments. We thank Dr. Xiao-Jiang Li and Shi-Hua Li at Jinan University for their generous help on monkey experiments. We thank all the technicians and core facility in the Analytical and Testing Center, Huazhong University of Science and Technology. This study is supported by the Major Project of "Brain Science and Brain-inspired Research" (2022ZD0211800), and National Natural Science Foundation of China (82030032, 32070960, 81871108, 31721002, 81829002), Top-Notch Young Talents Program of China of 2014 to Dr. Ling-Qiang Zhu.

AUTHOR CONTRIBUTIONS

LQZ and DL initiated and designed the study, DL, PF, YML, and HYM supervised the study; JZ performed the molecular biological experiments and animal experiments; CL performed the electrophysiology experiments; JZ, ZQL, and CQY performed animal experiments; WLY provided the monkey brains. DL, LQZ, PF, HYD, JW, WDB, HYM, YL, and KC provide experimental guide; JZ, WDB, FH and LQZ analyzed the data; LQZ and JZ wrote the manuscript.

COMPETING INTERESTS

The authors declare no competing interests.

ADDITIONAL INFORMATION

Supplementary information The online version contains supplementary material available at https://doi.org/10.1038/s41380-022-01694-5.

Correspondence and requests for materials should be addressed to Ling-Qiang Zhu.

Reprints and permission information is available at http://www.nature.com/reprints

Publisher's note Springer Nature remains neutral with regard to jurisdictional claims in published maps and institutional affiliations.